

Dalton Transactions

Accepted Manuscript



This is an *Accepted Manuscript*, which has been through the RSC Publishing peer review process and has been accepted for publication.

Accepted Manuscripts are published online shortly after acceptance, which is prior to technical editing, formatting and proof reading. This free service from RSC Publishing allows authors to make their results available to the community, in citable form, before publication of the edited article. This *Accepted Manuscript* will be replaced by the edited and formatted *Advance Article* as soon as this is available.

To cite this manuscript please use its permanent Digital Object Identifier (DOI®), which is identical for all formats of publication.

More information about *Accepted Manuscripts* can be found in the [Information for Authors](#).

Please note that technical editing may introduce minor changes to the text and/or graphics contained in the manuscript submitted by the author(s) which may alter content, and that the standard [Terms & Conditions](#) and the [ethical guidelines](#) that apply to the journal are still applicable. In no event shall the RSC be held responsible for any errors or omissions in these *Accepted Manuscript* manuscripts or any consequences arising from the use of any information contained in them.

Determination of chemical affinity of graphene oxide nanosheets with radionuclides investigated by macroscopic, spectroscopic and modeling techniques

Congcong Ding¹, Wenchai Cheng², Yubing Sun^{1*}, Xiangke Wang^{1*}

Abstract: The chemical affinity of graphene oxide (GO) nanosheets with radionuclides (Eu(III) and U(VI)) was determined by macroscopic, spectroscopic and modeling techniques. The macroscopic results showed that the adsorption of Eu(III) and U(VI) on GO nanosheets was independent of ionic strength, indicating that inner-sphere surface complexation predominated their adsorption. The maximum adsorption capacities calculated from Langmuir model at pH 4.0 and $T = 303$ K were 208.33 mg U(VI) and 28.70 mg Eu(III) per gram of GO nanosheets, respectively. No hysteresis was observed for both Eu(III) and U(VI) on GO nanosheets when desorption was initiated by lowering solution pH. While desorption was induced by replacing the radionuclide supernatant liquid with radionuclide-free electrolyte solution, the adsorption-desorption hysteresis was observed for U(VI) but not for Eu(III), indicating that the chemical affinity of GO nanosheets with U(VI) was stronger than that of GO nanosheets with Eu(III). The adsorption behaviors of Eu(III) and U(VI) on GO nanosheets can be fitted by double diffuse layer surface

¹ Key Lab of Novel Thin Film Solar Cells, Chinese Academy of Sciences, P.O. Box 1126, Hefei, 230031, P.R. China. E-mail address: sunyb@ipp.ac.cn (Y. Sun), Tel.: +86551 5592788; Fax: +86 551 5591310.

² School of Life Science, Sichuan University, Chengdu, 610064, P.R. China

complexation model with the mononuclear monodentate $>\text{SOM}^{(n-1)+}$ and $>\text{SOMOH}^{(n-2)+}$ complexes, and larger log K values of U(VI) was observed as compared to those of Eu(III). According to the spectroscopic analysis, the irreversible adsorption of U(VI) on GO nanosheets at variable radionuclide concentrations was attributed to the oxygen-containing functional groups.

Keywords: Graphene oxide, Radionuclides, Interaction mechanism, XPS

1. Introduction

Treatment of the contaminated groundwater containing radionuclides has become an essential task in the clean-up of legacy nuclear sites¹. Radionuclides released into environment pose a long-time threat to human beings and bio-organism, especially those long-lived radionuclides. In recent years, the studies on the removal of radionuclides from aqueous solutions have been extensively studied by using kinds of adsorbents such as clay minerals^{2, 3}, metal oxides⁴, and carbon materials⁵. In these studies, various environmental factors (i.e., pH, ionic strength and solution concentration) on radionuclide adsorption were investigated by batch techniques. However, these materials either suffer from low adsorption capacities or weak chemical stabilities under various environmental conditions. Hence, highly efficient enrichment of radionuclides from aqueous solution is needed for sustainable development of nuclear energy and cleanup in environmental management.

Due to the high surface area, strong reactive sites, and abundant functional groups on the surfaces, graphene oxide (GO) nanosheets have been demonstrated the effective removal of heavy metals⁶⁻⁸ and radionuclides⁹⁻¹³. Sun et al.¹¹ found the high

adsorption of Eu(III) ($175.44 \text{ mg}\cdot\text{g}^{-1}$) on GO nanosheets at pH 6.0. Romanchuk et al.¹⁰ also demonstrated that the GO presented high adsorption capacity for radionuclides such as $35 \text{ }\mu\text{mol Am(III)}$ and $97 \text{ }\mu\text{mol U(VI)}$ per gram of GO at pH 3.5. However, little literatures on the desorption of U(VI) and Eu(III) from GO nanosheets are available. The understanding of the desorption behaviors under various environmental factors is essential to evaluate the feasibility of GO nanosheets as promising materials for the removal of radionuclides from aqueous solutions in wastewater treatment^{14, 15}. Therefore, the desorption behavior is of great importance to assess health risks of radionuclides released into environment. Moreover, the desorption behaviors are conducive to understand the interaction mechanism between radionuclides and GO nanosheets.

Surface complexation modeling has been proven as one of the most powerful techniques for interpreting the interaction mechanism between adsorbate and adsorbents¹⁶. The selection of surface complexation modeling corresponding thermodynamic constants is based on structural data gained from spectroscopic technique. Various surface complexation models such as the constant capacitance model, double diffuse model and triple layer model have been extensively studied to simulate the adsorption behaviors of metal ions¹⁷⁻¹⁹. However, different surface complexes have been proposed to occur depending on the various chemical environments such as pH, ionic strength, and temperatures. Results obtained by surface complexation modeling using these approaches can be compared with the results of spectroscopic approaches such as extended X-ray absorption fine structure

spectroscopy and X-ray photoelectron spectroscopy. Hence, a thorough understanding of the adsorption processes of radionuclides on GO nanosheets by using surface complexation models is significant to interpret their interaction mechanism.

The purposes of this study are: (1) to elaborate the effect of pH, ionic strength, solution concentration, and temperature on radionuclides adsorption-desorption on GO nanosheets; (2) to simulate the adsorption behavior of radionuclides on GO nanosheets by using surface complexation model; and (3) to explore the adsorption mechanism between radionuclides and GO nanosheets in terms of X-ray photoelectron spectroscopy (XPS) analysis; This paper focuses on the interaction mechanism between radionuclides and GO nanosheets by combining with macroscopic, spectroscopic and modeling technique.

2. Experimental

2.1 The preparation and characterization of GO nanosheets

The GO nanosheets were synthesized by the modified Hummers method²⁰. Typically, flake graphite and NaNO₃ (as co-solvent) were added into concentrated H₂SO₄ under stirring conditions, the oxidizing agent (KMnO₄) was slowly added into the suspension, and the residual MnO₄⁻ was reduced by using reducing agent (30 v/v % H₂O₂). The GO nanosheets were obtained by centrifuging it at 18000 rpm for 60 min after ultrasonic treatment several times. More details on the synthesis and characterization of GO nanosheets can be found in our previous literatures^{6, 11}.

2.2 Batch adsorption and desorption experiments

The adsorption experiments as a function of pH, ionic strength, solution concentration

and temperature were conducted in polycarbonate tubes under N_2 conditions by the batch technique. The pH of suspension was adjusted from pH 2.0 to 10.0 by the drop wise addition of the negligible amount of 0.1 mol/L $HClO_4$ or NaOH solutions. The isothermal adsorption of radionuclides on GO nanosheets was investigated at pH 4.0 with the initial concentration of Eu(III) and U(VI) range from 5 to 60 mg/L, respectively. The suspensions were then sealed under N_2 (g) conditions and continuously stirred for 2 days to achieve adsorption equilibrium. The solid phase was separated from solution phase by centrifugation at 18000 rpm for 30 min.

Desorption experiments were caused by two ways: (1) by lowering the solution pH with acid, (2) by replacing the radionuclide supernatant liquid with radionuclide-free electrolyte solution with the aim to lower radionuclide concentration. Desorption by lowering solution pH was conducted using a method similar to Gao et al.²¹ by first preparing several samples for Eu(III) and U(VI) adsorption on GO nanosheets, and then making these samples equilibrate at certain pH values. Then the negligible amount of $HClO_4$ was added to these samples to lower the solution pH, allowing the solution to re-equilibrate before analyzing for the solution-phase radionuclide concentrations. For the desorption by replacing radionuclide supernatant after the adsorption isotherm experiments, a half volume of the supernatant of solutes after equilibrium was displaced by the equivalent volume of radionuclide-free background electrolyte solution with the same pH values. After the equilibrium of the suspension, the supernatants were measured to calculate the residual concentrations of radionuclides on GO nanosheets by mass balance.

The concentrations of radionuclide $^{152}\text{Eu(III)}$ were analyzed by liquid scintillation counting using a Packard 3100 TR/AB liquid scintillation analyzer (Perkin Elmer) with the scintillation cocktail (ULTIMA GOLD ABTM, Packard), and the amount of U(VI) was measured by kinetic phosphorescence analyzer (KPA-11, Richland, USA). The removal percentage of radionuclide (adsorption (%)) and adsorption capacity (Q_s , mg/g) can be expressed as Eqs. (1) and (2), respectively:

$$\text{adsorption (\%)} = (C_0 - C_{eq}) / C_0 \times 100\% \quad (1)$$

$$Q_s = V \times (C_0 - C_{eq}) / m \quad (2)$$

where C_0 (mg/L) and C_{eq} (mg/L) are initial concentration and concentration after adsorption, respectively. m (g) and V (mL) are the mass of GO nanosheets and the volume of the suspension, respectively. All experimental data were the average of triplicate determinations and the relative errors were within $\pm 5\%$.

2.3 Langmuir and Freundlich models

The Langmuir isotherm model is commonly used to describe monolayer adsorption process onto a surface, while the Freundlich isotherm model, an empirical expression, depicts the heterogeneous adsorption with exponential distribution of the sites and their energies²². The linear forms of Langmuir and Freundlich equation can be expressed as Eqs. (3) and (4), respectively:

$$C_{eq}/Q_s = 1/(b \times Q_{max}) + C_{eq}/Q_{max} \quad (3)$$

$$\log Q_s = \log K_F + 1/n \times \log C_{eq} \quad (4)$$

where Q_{max} (mg/g) is the maximum adsorption capacity of adsorbent at complete monolayer coverage. b (L/mg) is a Langmuir constant, which is related to the free

energy of sorption. $1/n$ is the heterogeneity of the adsorption sites; K_F represents equilibrium coefficient, which describes the partitioning of the adsorbate between the solid and liquid phases over the concentration range studied.

2.4 Surface complexation modeling

The pH-dependent adsorption of Eu(III) and U(VI) onto GO nanosheets were fitted by the diffuse double layer model (DDLDM) with the aid of FITEQL v 4.0 codes²³. FITEQL program is an iterative, gradient-directed nonlinear least-squares optimization program based on the Gauss method, which is used extensively to fit data of potentiometric titration and adsorption^{17, 24-26}. The good fit can be evaluated by weighted sum of squares divided by degrees of freedom (WSOS/DF), which is indicated by a value of WSOS/DF between 0.1 and 20²³.

3. Results and Discussion

3.1 Batch adsorption experiments

3.1.1 Adsorption kinetics

The adsorption of Eu(III) and U(VI) on GO nanosheets as a function of contact time is shown in Fig. 1. It is clear that the adsorption process is rapid to reach equilibrium for Eu(III) and U(VI) within 30 min. Approximately 60 % of Eu(III) and 75 % of U(VI) are adsorbed on the GO nanosheets at pH 4.0 within 10 min of contact time. The open and flat structures of GO nanosheets guarantee the sufficient exposure of surface active sites, which may contribute to the rapid adsorption rate for Eu(III) and U(VI) on GO nanosheets. The short equilibrium time for the two radionuclides on GO nanosheets indicates that GO nanosheets can serve as the promising materials in

continuous waste water treatment.

In order to obtain useful information for confirming the underlying mechanisms during the entire adsorption process, the experimental kinetic data of Eu(III) and U(VI) on GO nanosheets are simulated by the pseudo-first order and pseudo-second order kinetic models. Their linear forms are given in Eqs. (5)²⁷ and (6)²⁸, respectively:

$$\ln(q_e - q_t) = \ln q_e - k_f \times t \quad (5)$$

$$t/q_t = 1/(k_s \times q_e^2) + t/q_e \quad (6)$$

where q_e and q_t (mg/g) are the amount of radionuclides adsorbed at equilibrium and at time t , respectively. k_f and k_s are the pseudo-first order and pseudo-second order kinetic rate constant, respectively. As shown in Fig. 1, the adsorption of Eu(III) and U(VI) on GO nanosheets are well simulated by pseudo-second order kinetic model ($R^2 > 0.99$) compared to pseudo-first order ($R^2 < 0.45$, data not shown). The adsorption kinetics indicates that the adsorption of Eu(III) and U(VI) on GO nanosheets is the rate-limiting step²⁸. Ho et al.²⁹ also found that the adsorption of divalent metal ions on peat can be fitted by pseudo-second order kinetic model very well. The authors assumed that the adsorption kinetics is limited by the binding reaction itself and not the diffusion of species. chemisorption occurs involving valence forces through sharing or exchange of electrons between peat and divalent metal ions.

3.1.2 Effect of pH and ionic strength

The effect of pH on Eu(III) and U(VI) adsorption onto GO nanosheets was investigated by batch technique (Fig. 2A and 2B). As illustrated in Fig. 2A and 2B,

Eu(III) adsorption increases from pH 2.0 to 6.0, and then keeps this level at pH 6.0-9.0. However, the adsorption of U(VI) on GO nanosheets increases sharply at pH 2.0- 4.5, then reaches a plateau and remains constant at pH 4.5-7, whereas the decreased adsorption is observed at pH > 7. The observed adsorption trends can be interpreted by the relative distribution of Eu(III) and U(VI) in respective solution and the surface property of GO nanosheets. Fig. 2C and 2D illustrate the correspondingly relative proportion of Eu(III) and U(VI) species in solution with absence of GO nanosheets, computed by PHREEQC³⁰. It is clear that Eu^{3+} is the main species of Eu(III) aqueous solution at pH < 5.0, then, with increase in pH, the hydrolyzed mononuclear and multinuclear species increase (i.e., $\text{Eu}(\text{OH})^{2+}$, $\text{Eu}_2(\text{OH})_2^{4+}$). The precipitate $\text{Eu}(\text{OH})_3$ appear at pH 8.0. According to the analysis of potentiometric acid-base titration, the pH_{PZC} of GO nanosheets is 4.5, so the charge of GO nanosheets is negative at pH > 4.5. Therefore, the positive Eu(III) species are easily to be adsorbed on negatively charged GO nanosheets due to the electrostatic attraction. It is worth noting that with increasing pH, variable Eu(III) species may form different complex with GO nanosheets. Our previous studies using EXAFS analysis found that Eu(III) formed mononuclear monodentate complexes at pH 6.3 and multinuclear surface complexes at pH 9.0¹¹. It was also found that the coordination number and bond distance of first coordination shell (Eu–O path) decreased from ~ 9.94 to ~ 8.56 and 2.415 \AA to 2.360 \AA , respectively with increasing pH². In addition, the high level adsorption of Eu(III) on GO nanosheets can also be attributed to partial precipitation/co-precipitation of Eu(III) at pH > 8.0. As shown in Fig. 2D, the predominate species

of U(VI) in aqueous solution are UO_2^{2+} at $\text{pH} < 4.0$, and more complex hydrolyzed species (e.g., UO_2OH^+ , $(\text{UO}_2)_3(\text{OH})_5^+$ and $(\text{UO}_2)_4(\text{OH})_7^+$, $\text{UO}_2(\text{OH})_2$) are observed at $\text{pH} 4.0\text{-}9.0$. However, being different from Eu(III), the negatively charged U(VI) species (i.e., $\text{UO}_2(\text{OH})^-$ and $(\text{UO}_2)_3(\text{OH})_7^-$) arise at $\text{pH} > 7.0$. The suppressed adsorption of U(VI) on GO nanosheets at $\text{pH} > 7.0$ is due to the electrostatic repulsion between negative GO nanosheets and negative U(VI) species. It is worthy to note that the pH-dependent adsorption edge of U(VI) on GO nanosheets shifts to the lower pH conditions compared to that of Eu(III), indicating the high affinity of U(VI) to GO nanosheets.

The effect of ionic strength on Eu(III) and U(VI) adsorption onto GO nanosheets is also shown in Fig. 2A and 2B. Little effect of ionic strength on Eu(III) and U(VI) adsorption onto GO nanosheets is observed, which is consistent with the results of Sun et al.¹¹. Zhao et al.⁶ also found the adsorption of Co(II) and Cd(II) on GO nanosheets was independent of ionic strength at high pH conditions. The adsorption mechanism, including outer-sphere and inner-sphere surface adsorption, can be demonstrated by the effect of ionic strength³¹. The outer-sphere surface adsorption is assumed to occur primarily on permanent charge sites via cation exchange resulting from the attraction by the negative potential, which is strong influenced by the concentration of ionic strength. However, the inner-sphere surface complexes are formed by the complexation of adsorbate with amphoteric groups by chemical bond, which is less ionic strength-dependent^{2, 32-34}. Therefore, the little effect of ionic strength on the removal of adsorptive ions is inner-sphere surface complexation,

whereas the strong effect of ionic strength on the removal of adsorptive ions is outer-sphere surface complexation³⁵. Little effect of ionic strength on Eu(III) and U(VI) adsorption onto GO nanosheets is observed, revealing that the adsorption of Eu(III) and U(VI) adsorption onto GO nanosheets is predominately inner-sphere surface complexation. In addition, our XPS results also reveal the shift of binding energy and the decrease of peak area of O 1s spectra after adsorption, suggesting the adsorption of Eu(III) and U(VI) on GO nanosheets is combined by chemical bond. It might be the plentiful oxygen-containing functional groups on GO nanosheets that contribute the formation of strong complexes between Eu(III) or U(VI) ions and GO nanosheets, and contribute the inner-sphere adsorption.

3.1.3 Adsorption isotherms and thermodynamic data.

Adsorption isotherms of Eu(III) and U(VI) on GO nanosheets are displayed in Fig. 3. As shown in Fig. 3, the adsorption of Eu(III) and U(VI) on GO nanosheets increases with increasing solution concentration. It is also observed that the amounts of U(VI) adsorbed on GO nanosheets are much larger than that of Eu(III) at pH 4.0. The adsorption isotherms of Eu(III) and U(VI) are also fitted by Langmuir and Freundlich models, and their relative parameters calculated from the two models are listed in Table 1. As tabulated in Table 1, one can see that the adsorption of Eu(III) and U(VI) on GO nanosheets can be better fitted by Langmuir model ($R^2 > 0.995$) than Freundlich model, suggesting that the adsorption of Eu(III) and U(VI) on GO nanosheets are monolayer adsorption. The maximum adsorption capacities of GO nanosheets calculated from Langmuir model at pH 4.0 and $T = 303$ K are 208.33 mg/g

for U(VI) and 28.70 mg/g for Eu(III), whereas the higher adsorption capacity of GO nanosheets for Eu(III) (175 mg/g) was reported by Sun et al.¹¹ who was conducted it at higher pH (6.0) conditions. The higher adsorption capacity of GO nanosheets for U(VI) could be attributed to the stronger chemical affinity of GO nanosheets with U(VI) at low pH conditions compared to Eu(III), which is consistent with the results of pH-dependent adsorption.

The effect of temperature on Eu(III) and U(VI) adsorption isotherms on GO nanosheets at pH 4.0 is also given in Fig. 3. For both Eu(III) and U(VI), adsorption capacity is the highest at $T = 333$ K and the lowest at $T = 303$ K, showing that both Eu(III) and U(VI) adsorption on GO nanosheets are promoted at higher temperature.

The thermodynamic parameters (standard free energy change- ΔG^0 , standard enthalpy change- ΔH^0 and the standard entropy change- ΔS^0) can be calculated from the temperature dependent adsorption isotherms. The ΔG^0 can be calculated from Eq. (7):

$$\Delta G^0 = -RT \ln K^0 \quad (7)$$

where R is the universal constant (8.314 J/(mol*K)) and T is the temperature of Kelvin.

The sorption equilibrium constant K^0 can be calculated by plotting $\ln K_d$ versus C_e and extrapolating C_e to zero.

The ΔH^0 and ΔS^0 can be calculated according to Eq. (8):

$$\ln K^0 = \Delta S^0/R - \Delta H^0/RT \quad (8)$$

The thermodynamic parameters of Eu(III) and U(VI) adsorption on GO nanosheets are tabulated in Table 2. The negative ΔG^0 values indicate that the adsorption of Eu(III) and U(VI) on GO nanosheets are spontaneous processes. The value of ΔG^0 decreases

with increasing temperature, indicating that the higher adsorption is observed at higher temperature. It is also worth to note that the ΔG^0 value of U(VI) is lower than that of Eu(III) at different temperatures, suggesting the higher adsorption of U(VI) compared to that of Eu(III). The positive values of ΔH^0 (8.79 kJ/mol for Eu(III) and 9.88 kJ/mol for U(VI)) indicate that the adsorption of Eu(III) and U(VI) on the GO nanosheets are endothermic processes, which are in good agreement with the previous reports^{9, 11}. It is believed that the dehydration of metal ions from their aqueous complex is an endothermic process and is favored at high temperature³⁶, while attachment of metal ions on the surface of GO nanosheets is an exothermic process. Therefore, it is plausible that the energy of dehydration of radionuclides exceeds exothermicity of the attachment of radionuclides on the surface of GO nanosheets. This is an implicit assumption herein that the adsorbed Eu(III) and U(VI) are less hydrated than those in aqueous solution. The positive ΔS^0 value implies some structural changes in Eu(III) and U(VI) on GO nanosheets during the adsorption process, which leads to an increase in the disorder of the solid-solution system during the adsorption processes. Thus the positive ΔS^0 values also suggest that the adsorption of Eu(III) and U(VI) on GO nanosheets is spontaneous sorption process with high chemical affinity.

3.2 Batch desorption experiments

3.2.1 Desorption kinetics

The desorption kinetics of Eu(III) and U(VI) from GO nanosheets induced by lowering pH from pH 4.0 to 2.5 and by replacing radionuclide supernatant liquid

with radionuclide-free electrolyte solution are shown in Fig. 4A and 4B, respectively. As illustrated in Fig. 4A, the desorption of Eu(III) and U(VI) from GO nanosheets reach equilibrium within 5 min. However, their desorption induced by lowering radionuclide concentration need longer contact time (4 h) to reach equilibrium (as shown in Fig. 4B), which is consistent with the report of Um et al.³⁷. The data of desorption by the two methods indicated that the Eu(III) and U(VI) adsorption on GO nanosheets is influenced by the pH of aqueous solution. It was determined that the metal ion can be dissociated from surface complex at low pH³⁸⁻⁴¹: $\text{SOM}^{n+} + \text{H}^+ = \text{M}^{(n+1)+} + \text{SOH}$. Therefore, the Eu(III) and U(VI) are detached from the complexes at lower pH conditions. As shown in Fig. 4B, one also can be seen that the adsorbed Eu(III) and U(VI) are released into liquid solution when the concentration of Eu(III) and U(VI) is lowered (Fig. 4B). However, the decreased adsorption induced by lowering radionuclide concentration is ignored compared with that of induced by lowering pH. The initial pH controls efficiency of adsorbate removal rather than initial metal concentration⁴².

3.2.2 Desorption initiated by lowering solution pH

The desorption edges (i.e., the percent of Eu(III) and U(VI) left on GO nanosheets after desorption by lowering solution pH) are shown in Fig. 5A and 5B. Desorption edges of Eu(III) and U(VI) are almost identical to their respective adsorption edges, suggesting that their adsorption on GO nanosheets is completely reversible when desorption is caused by lowering solution pH. Gao et al.²¹ also found the reversible adsorption of Cd(II) and Pb(II) on Utica sediments when lowering solution pH, and

they concluded that the reversible adsorption might result from the formation of pH-dependent surface polymer of metal at the adsorbents. As discussed previous, pH in aqueous solution presents an obvious effect on dissolution of surface complexes: $SOM^{n+} + H^+ = M^{(n+1)+} + SOH$, therefore the desorbed amounts of Eu(III) and U(VI) from surface complexes increase with decreasing pH. The dissolution of surface complexes appear to be associated with the species of surface complexes: that mononuclear ligand surface complexes enhanced but multinuclear surface complexes inhibited the dissolution of surface complexes³⁸. It was believed that the mononuclear surface complexes is formed when pH is lowered, thereby enhancing the dissolution of Eu(III) and U(VI) from the corresponding surface complexes and decreasing the adsorption of Eu(III) and U(VI) on GO nanosheets.

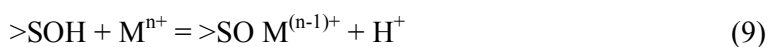
3.2.3 Desorption initiated by replacing the radionuclide supernatant with radionuclide-free electrolyte solution

The desorption isotherms (desorption induced by replacing radionuclide supernatant) of Eu(III) and U(VI) from GO nanosheets are shown in Fig. 5C and 5D. As shown in Fig. 5D, the desorption isotherm of U(VI) from GO nanosheets significantly deviates from its adsorption isotherm, indicating the adsorption-desorption hysteresis. The results are consistent with the findings of Gao et al.²¹ who determined that adsorption-desorption hysteresis of Cd(II) and Pb(II) on Utica sediments was observed by using the replaced electrolyte solution method. The adsorption-desorption hysteresis can be divided into two types: reversible and irreversible hysteresis⁴³. The reversible hysteresis is complete desorption without intervention,

appearing as a closed hysteresis loop between desorption and adsorption curves. The irreversible hysteresis means that complete desorption cannot happen without intervention (e.g., vigorous solvent extraction)⁴⁴. Fig. 5D shows that the desorption of U(VI) from GO nanosheets is irreversible process. Yin et al.⁴⁵ found that mercury (Hg(II)) desorption from 15 soils exhibited the obvious hysteresis. Undabeytia et al.⁴⁶ reported that the desorption hysteresis of Cu(II) on planar sites of montmorillonite was a function of equilibrium partitioning, whereas in the case of the edge sites, the large affinity of Cu(II) for these positions resulted in the hysteresis. The desorption hysteresis of Pb(II) on zeolitized tuffs was also attributed to their significantly strong adsorption³⁷. However, no desorption hysteresis of Eu(III) on GO nanosheets is observed (Fig. 5C). Therefore, it may be reasonable to postulate that desorption hysteresis of U(VI) on GO nanosheets can be due to the higher binding affinity of GO nanosheets for U(VI) compared to Eu(III).

3.3 Surface complexation modeling

The adsorption of Eu(III) and U(VI) on GO nanosheets are fitted by diffuse double-layer model (DDLm) with the aid of FITEQL v4.0 code and the results are shown in Figure 6. We used Eu(III) and U(VI) species over the pH range from 2.0 to 9.0 to optimize the adsorption process of Eu(III) and U(VI) on GO nanosheets. The main adsorption reactions can be expressed as Eq. (9) and (10):



where >SOH represents the amphoteric hydroxyl groups on the surface of GO

nanosheets. M^{n+} refers to Eu(III) or U(VI) cations. The log K values are obtained by best fitting the adsorption data of Eu(III) and U(VI) on GO nanosheets (Table 3). The simulation is accepted among the uncertainty range, $0.1 < V_{WSOS/DF} < 20.0$. The fitting results show subtle differences with experimental data over pH range from 2.0 to 9.0, indicating that Eu(III) or U(VI) adsorption on GO nanosheets are well modeled by DDLM. It was found that value of log K of U(VI) is higher than that of Eu(III) (Table 3), which substantiates the higher adsorption capacity of U(VI) on GO nanosheets compared to Eu(III), which is consistent with the results of batch adsorption and desorption isotherms. As shown in Figure 6, the main $>SOM^{(n-1)+}$ and $>SOMOH^{(n-2)+}$ species are observed at low and high pH conditions, respectively.

3.4 Adsorption Mechanism

The XPS spectroscopy technique was used to determine the interaction mechanism between radionuclides and GO nanosheets. Fig. 7 shows the XPS spectra of survey and high resolution scans for the O 1s, C 1s, Eu 3d and U 4f of GO nanosheets before and after desorption induced by replacing the radionuclide supernatant with radionuclide-free electrolyte solution (i.e., denoted as GO-Eu1 and GO-Eu2; GO-U1 and GO-U2, respectively). The occurrence of Eu 3d is observed in GO-Eu1 and GO-Eu2 sample in terms of the survey spectra (Fig. 7A), which indicates that Eu(III) is chemical adsorption onto the surface of GO nanosheets⁴⁷. For GO-Eu1 sample, the shift of binding energy and the decrease of peak area of O 1s spectra (Table 4) are observed, indicating that the adsorption of Eu(III) on GO nanosheets is attributed to the oxygen-containing functional groups. For GO-Eu2 sample as compared to

GO-Eu1 sample, the apparent increase of the peak area of O 1s and the corresponding decrease of the peak area of Eu 3d are observed, which is consistent with the results reported by Wang et al.⁴⁷ who found that an apparent decrease in Hg 4f peak area and a corresponding increase in O 1s peak area for PANI-Hg with 1 mol/L HCl. The survey scans of XPS spectra clearly demonstrate the adsorption of Eu(III) on GO nanosheets is relevant to oxygen-containing functional groups.

Fig. 7B shows the high resolution scans of O 1s of GO, GO-Eu1 and GO-Eu2 samples. For GO-Eu1 sample, the lower binding energy of O 1s is observed. As illustrated in Table 4, the binding energy of O 1s in GO-Eu2 (532.86eV) is higher than that of O 1s in GO-Eu1 (530.56eV), which is due to the increase of negative charge of the oxygen atom in the coordinated GO nanosheets after desorption. The analysis of high resolution scans of O 1s shows that the high adsorption capacity of GO nanosheets can be attributed to the weak affinity of Eu(III) to oxygen-containing functional groups on GO nanosheets.

Eu 3d and U 4f spectra before and after desorption could be characterized with two doublet-peaks such as Eu 3d_{5/2} (at 1134/1137 eV⁴⁸) and Eu 3d_{3/2} (at 1165 eV) peaks for Eu 3d (Fig. 7C) and U 4f_{7/2} (at 382 eV⁴⁹) and U 4f_{5/2} (392 eV⁴⁹) for U 4f (Fig. 7D). As shown in Table 4, the binding energy of Eu 3d_{5/2} on GO-Eu2 is higher than that of Eu 3d_{5/2} on GO-Eu1 sample, while the lower relative intensity of Eu 3d_{5/2} on GO-Eu2 is observed. As shown in Fig. 7D, the occurrence of two U 4f 7/2 peaks in the high resolution XPS scans shows that U(VI) could be complexed with two types of binding sites on the GO nanosheets (denoted U₁ and U₂ binding sites). Wang et al.⁴⁷ also

found that the existence of two Hg 4f doublets (Hg_1 and Hg_2) in the high resolution XPS spectra of PANI containing mercury, indicating mercury could be complexed to two types of general binding sites. As tabulated in Table 4, the change of binding energy of U 4f (i.e., $\Delta U 4f_{5/2} = 0.3$ eV) is lower than that of Eu 3d (i.e., $\Delta Eu 3d_{5/2} = 2.5$ eV), indicating that the chemical affinity of U(VI) by oxygen-containing functional groups (e.g., hydroxyl and carboxyl group) is higher than that of Eu(III). The results of XPS spectra analysis further corroborates the irreversible adsorption of U(VI) on GO nanosheets at variable U(VI) concentration as compared to that of Eu(III), which is agreement with the results of the batch adsorption and desorption.

4. Conclusion

The chemical affinity of GO nanosheets for radionuclides was determined by using macroscopic, spectroscopic and modeling techniques. The batch adsorption results indicated that the adsorption capacity of GO nanosheets for U(VI) was higher than that of Eu(III). The inner-sphere surface complexation was determined by ionic strength-independent adsorption. Reversible adsorption of Eu(III) and U(VI) on GO nanosheets was observed when desorption was initiated by lowering pH, whereas the adsorption of U(VI) on GO nanosheets was irreversible when desorption was induced by lowering radionuclide concentration. The highly chemical affinity of GO nanosheets for U(VI) was demonstrated by the simulation of adsorption data with DDLM modeling and analysis of XPS spectra. The significant potential of GO nanosheets was regarded as one of suitable materials for the preconcentration and removal of radionuclides in environmental pollution cleanup and nuclear waste

management.

Acknowledgments

Financial support from 973 projects from Ministry of Science and Technology of China (2011CB933700), National Natural Science Foundation of China (21207135, 21007074, 21207136, 21225730 and 91126020) and Hefei Center for Physical Science and Technology (2012FXZY005) are acknowledged.

References

- 1 K. Foo and B. Hameed, *Desalin. Water. Treat.* 2012, **41**, 72-78.
- 2 Q. Fan, X. Tan, J. Li, X. Wang, W. Wu and G. Montavon, *Environ. Sci. Technol.*, 2009, **43**, 5776-5782.
- 3 B. Fonseca, H. Figueiredo, J. Rodrigues, A. Queiroz and T. Tavares, *Geoderma*, 2011, **164**, 232-237.
- 4 X. Tan, Q. Fan, X. Wang and B. Grambow, *Environ. Sci. Technol.*, 2009, **43**, 3115-3121.
- 5 X. Tan, M. Fang, C. Chen, S. Yu and X. Wang, *Carbon*, 2008, **46**, 1741-1750.
- 6 G. Zhao, J. Li, X. Ren, C. Chen and X. Wang, *Environ. Sci. Technol.*, 2011, **45**, 10454-10462.
- 7 S. Yang, Y. Chang, H. Wang, G. Liu, S. Chen, Y. Wang, Y. Liu and A. Cao, *J. Colloid Interface Sci.*, 2010, **351**, 122-127.
- 8 R. Sitko, E. Turek, B. Zawisza, E. Malicka, E. Talik, J. Heimann, A. Gagor, B. Feist and R. Wrzalik, *Dalton Trans.*, 2013, **42**, 5682-5689.
- 9 Z. Li, F. Chen, L. Yuan, Y. Liu, Y. Zhao, Z. Chai and W. Shi, *Chem. Eng. J.*, 2012, **210**, 539-546.
- 10 A. Y. Romanchuk, A. S. Slesarev, S. N. Kalmykov, D. V. Kosynkin and J. M. Tour, *Phys. Chem. Chem. Phys.*, 2013, **15**, 2321-2327.
- 11 Y. Sun, Q. Wang, C. Chen, X. Tan and X. Wang, *Environ. Sci. Technol.*, 2012, **46**, 6020-6027.
- 12 G. Zhao, T. Wen, X. Yang, S. Yang, J. Liao, J. Hu, D. Shao and X. Wang, *Dalton Trans.*, 2012, **41**, 6182-6188.
- 13 Y. Sun, D. Shao, C. Chen, S. Yang and X. Wang, *Environ. Sci. Technol.*, 2013, **47**, 9904-9910.
- 14 M. S. Mauter and M. Elimelech, *Environ. Sci. Technol.*, 2008, **42**, 5843-5859.
- 15 W. Wu, W. Chen, D. Lin and K. Yang, *Environ. Sci. Technol.*, 2012, **46**, 5446-5454.
- 16 D. A. Kulik, S. U. Aja, V. A. Sinitsyn and S. A. Wood, *Goechim. Cosmochim. Acta*, 2000, **64**, 195-213.
- 17 K. F. Hayes, G. Redden, W. Ela and J. O. Leckie, *J. Colloid Interface Sci.*, 1991, **142**, 448-469.
- 18 R. P. Deo, W. Songkasiri, B. E. Rittmann and D. T. Reed, *Environ. Sci. Technol.*, 2010, **44**, 4930-4935.
- 19 X. Gu, L. J. Evans and S. J. Barabash, *Goechim. Cosmochim. Acta*, 2010, **74**, 5718-5728.
- 20 M. Hirata, T. Gotou, S. Horiuchi, M. Fujiwara and M. Ohba, *Carbon*, 2004, **42**, 2929-2937.
- 21 Y. Gao, A. T. Kan and M. B. Tomson, *Environ. Sci. Technol.*, 2003, **37**, 5566-5573.

- 22 W. Stumm, *Chemistry of the solid-water interface: Processes at the mineral-water and particle-water interface in natural systems*, John Wiley and Son Inc., New York, 1992.
- 23 A. Herbelin and J. Westall, *FITEQL 4.0: A computer program for determination of chemical equilibrium constants from experimental data*. Department of Chemistry, Oregon State University, Corvallis, OR, 1999.
- 24 M. O. Barnett, P. M. Jardine and S. C. Brooks, *Environ. Sci. Technol.*, 2002, **36**, 937-942.
- 25 C. L. Peacock and D. M. Sherman, *Goechim. Cosmochim. Acta.*, 2004, **68**, 2623-2637.
- 26 W. Um, R. J. Serne and K. M. Krupka, *Environ. Sci. Technol.*, 2007, **41**, 3587-3592.
- 27 S. Lagergren, *K. Sven. Vetenskapsakad. Handl.*, 1898, **24**, 1-39.
- 28 Y.-S. Ho, *J. Hazard. Mater.*, 2006, **136**, 681-689.
- 29 Y.-S. Ho, W.-T. Chiu, C.-S. Hsu and C.-T. Huang, *Hydrometallurgy*, 2004, **73**, 55-61.
- 30 D. L. Parkhurst and C. Appelo, *User's guide to PHREEQC (Version 2)—A computer program for speciation, batch-reaction, onedimensional transport, and inverse geochemical calculations: U.S. Geological Survey Water-Resources Investigations Report*, 1999.
- 31 D. G. Strawn and D. L. Sparks, *J. Colloid Interface Sci.*, 1999, **216**, 257-269.
- 32 T. Rabung, M. Pierret, A. Bauer, H. Geckeis, M. Bradbury and B. Baeyens, *Goechim. Cosmochim. Acta*, 2005, **69**, 5393-5402.
- 33 V. Sinityn, S. Aja, D. Kulik and S. Wood, *Goechim. Cosmochim. Acta*, 2000, **64**, 185-194.
- 34 C. Papelis and K. F. Hayes, *Colloid. Surface. A.*, 1996, **107**, 89-96.
- 35 J. Zachara, S. Smith, J. McKinley and C. Resch, *Soil Sci. Soc. Am. J.*, 1993, **57**, 1491-1501.
- 36 S. Tahir and N. Rauf, *J. Chem. Thermodyn.*, 2003, **35**, 2003-2009.
- 37 W. Um and C. Papelis, *Environ. Sci. Technol.*, 2004, **38**, 496-502.
- 38 W. Stumm, *Aquatic Chemistry. American Chemical Society, Washington, DC*, 1995, 1-32.
- 39 J. Galvez, M. L. Alcaraz, T. Perez and M. H. Cordoba, *Anal. Chem.*, 1985, **57**, 2116-2120.
- 40 M. S. Shuman and G. P. Woodward Jr, *Anal. Chem.*, 1973, **45**, 2032-2035.
- 41 B. J. Fuhr and D. L. Rabenstein, *Inorg. Chem.*, 1973, **12**, 1868-1874.
- 42 Y. Ho, D. John Wase and C. Forster, *Water Res.*, 1995, **29**, 1327-1332.
- 43 A. S. Gunasekara and B. Xing, *J. environ. qual.*, 2003, **32**, 240-246.
- 44 A. Kan, G. Fu, M. Hunter, W. Chen, C. Ward and M. Tomson, *Environ. Sci. Technol.*, 1998, **32**, 892-902.
- 45 Y. Yin, H. E. Allen, C. Huang and P. F. Sanders, *Soil. Sci.*, 1997, **162**, 35-45.
- 46 T. Undabeytia, S. Nir, G. Rytwo, C. Serban, E. Morillo and C. Maqueda, *Environ. Sci. Technol.*, 2002, **36**, 2677-2683.
- 47 J. Wang, B. Deng, H. Chen, X. Wang and J. Zheng, *Environ. Sci. Technol.*, 2009, **43**, 5223-5228.
- 48 A. Kowal-Fouchard, R. Drot, E. Simoni, N. Marmier, F. Fromage and J.-J. Ehrhardt, *New. J. Chem.*, 2004, **28**, 864-869.
- 49 T. Ejima, S. Sato, S. Suzuki, Y. Saito, S. Fujimori, N. Sato, M. Kasaya, T. Komatsubara, T. Kasuya and Y. Ōnuki, *Phys. Rev. B*, 1996, **53**, 1806.

Figure captions

Figure 1 Adsorption kinetics of Eu(III) and U(VI) on GO nanosheets, $C_0 = 10.0$ mg/L, pH = 4.0, m/V = 0.20 g/L, $I = 0.01$ mol/L NaClO₄, $T = 303$ K. the inserted curve: the fitting of pseudo-second order kinetic model.

Figure 2 Effect of pH and ionic strength on the adsorption of A: Eu(III) and B: U(VI) onto GO nanosheets; speciation of C: Eu(III) and D: U(VI) in NaClO₄ solution, $C_0 = 10.0$ mg/L, m/V = 0.20 g/L, $T = 303$ K, $I = 0.01$ mol/L NaClO₄.

Figure 3 Adsorption isotherms of A: Eu(III) and B: U(VI) on GO nanosheets at different temperatures, pH = 4.0, m/V = 0.20 g/L, $I = 0.01$ mol/L NaClO₄.

Figure 4 Desorption kinetics of Eu(III) and U(VI) from GO nanosheets, A: desorption by lowering pH from 4.0 to 2.5, m/V = 0.20 g/L, $T = 303$ K, $I = 0.01$ mol/L NaClO₄; B: desorption by replacing radionuclide supernatant method, pH=4.0, $C_0 = 10.0$ mg/L, m/V = 0.20 g/L, $T = 303$ K, $I = 0.01$ mol/L NaClO₄.

Figure 5 Adsorption and desorption of Eu(III) and U(VI) from GO nanosheets, m/V = 0.20 g/L, $T = 303$ K, $I = 0.01$ mol/L NaClO₄. by lowering solution pH, A: Eu(III); B: U(VI), $C_0 = 10.0$ mg/L; and by replacing radionuclide supernatant method C: Eu(III); D: U(VI), pH = 4.0.

Figure 6 Simulation of adsorption with diffuse double-layer model (DDLm), A: Eu(III); B: U(VI), $C_0 = 10.0$ mg/L, m/V = 0.20 g/L, $I = 0.01$ mol/L NaClO₄, $T = 303$ K.

Figure 7 The survey scan and high resolution scans of XPS analysis of GO nanosheets before and after desorption by replacing radionuclide supernatant method.

(A): total survey scans; (B): O 1s peaks; (C): Eu 3d peaks, (D): U 4f peaks, $m/V =$

0.20 g/L, pH = 4.0, $I = 0.01$ mol/L NaClO₄

Figures

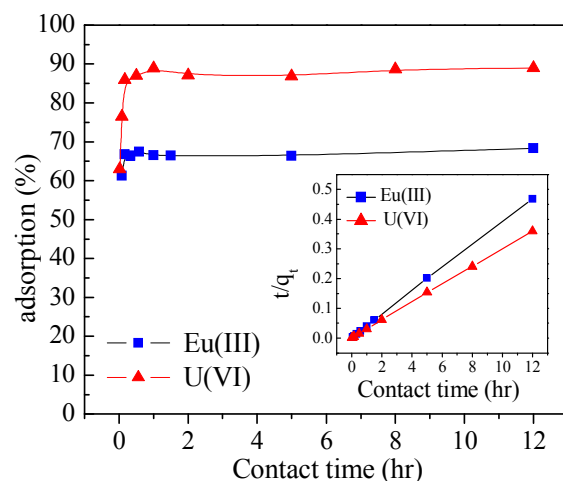


Fig. 1

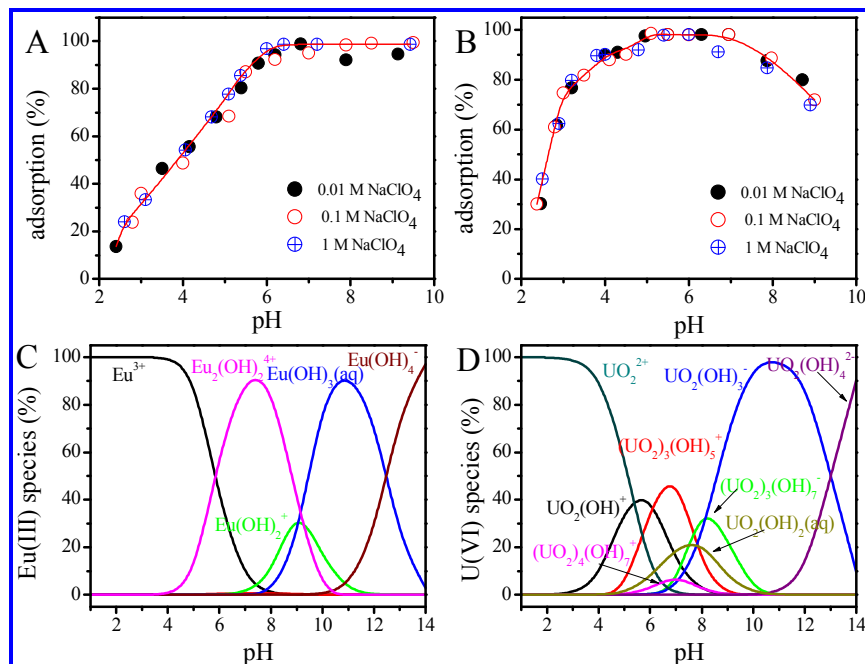


Fig. 2

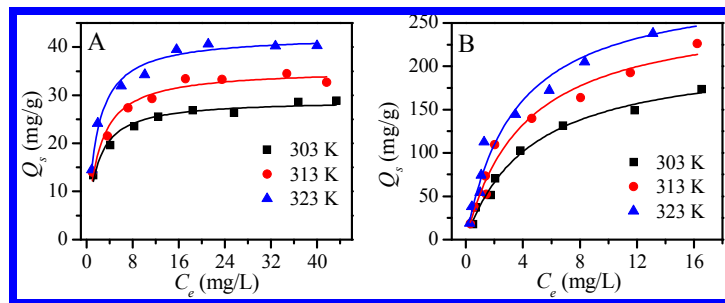


Fig. 3

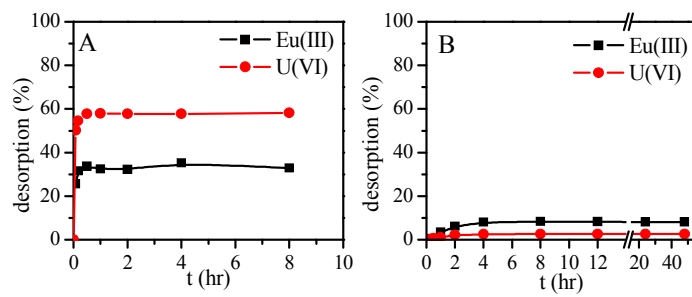


Fig. 4

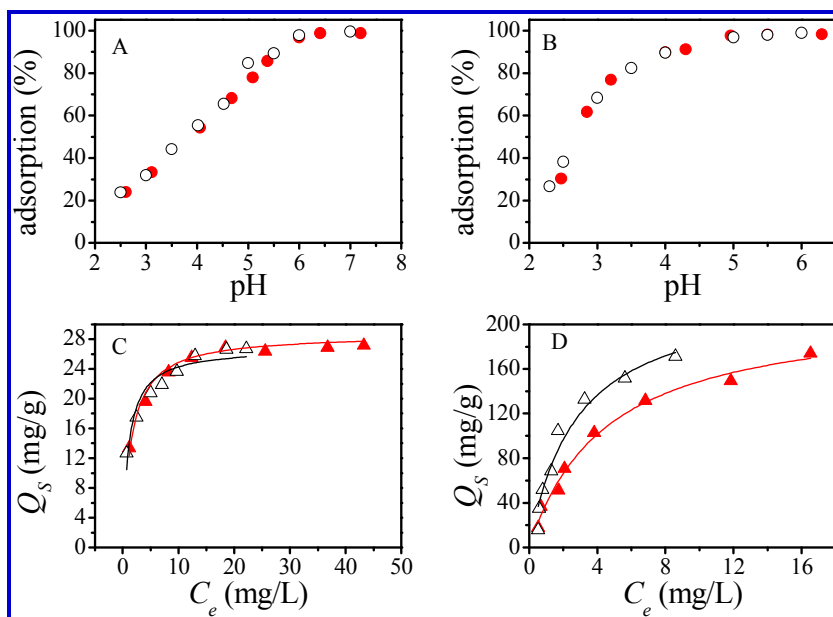


Fig. 5

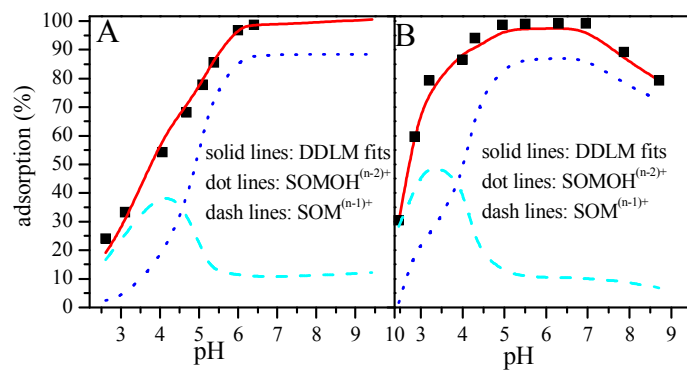


Fig. 6

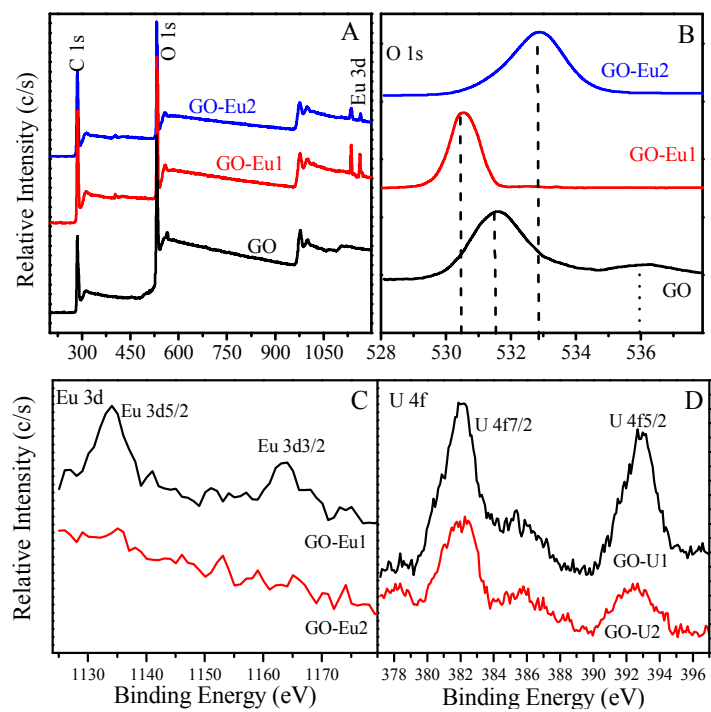


Fig. 7

Tables

Table 1. Parameters of adsorption models for radionuclides on GO nanosheets.

Adsorbate	Langmuir			Freundlich		
	b (L/mmg)	Q_{max} (mg/g)	R^2	$\ln K_F$ (mg/g)/(mg/L) ⁿ	$1/n$	R^2
Eu(III)	0.7398	28.70	0.9979	2.6500	0.2027	0.9009
U(VI)	0.2637	208.33	0.9966	3.8764	0.4819	0.9792

Table 2. Thermodynamic parameters for radionuclides adsorption on GO nanosheets

$T(K)$	ΔG^0 (kJ/mol)		ΔS^0 (J/mol/K)		ΔH^0 (kJ/mol)	
	U	Eu(III)	U(VI)	Eu(III)	U(VI)	Eu(III)
303	-11.42	-9.01				
313	-11.78	-9.55	70.35	58.70	9.88	8.79
323	-12.93	-10.51				

Table 3. Parameters for the fitting of the adsorption of radionuclides on GO nanosheets

Specific Surface Area (S_{BET} , $\text{m}^2 \cdot \text{g}^{-1}$)	140.8
pH_{PZC} ^a	4.5
Surface site density ($\text{sites} \cdot \text{nm}^{-2}$)	29.08
Log K	4.23(Eu(III)) 4.62(U(VI))

^a data from acid-base titration.

Table 4. The Binding Energies of GO nanosheets before and after desorption by replaced radionuclide supernatant method.

Adsorbents	O 1s	Eu 3d _{5/2}	Eu 3d _{3/2}	U 4f _{7/2}	U 4f _{5/2}
GO	531.57				
GO-Eu1	530.56	1134.9	1164.3		
GO-Eu2	532.86	1137.4	1164.7		
GO-U1	532.01			382.28	392.38
GO-U2	531.98			382.28	392.68

